Impact of disorder on dynamics and ordering in the honeycomb-lattice iridate Na₂IrO₃



(Received 20 September 2019; accepted 22 January 2020; published 3 February 2020)

Kitaev's honeycomb spin-liquid model and its proposed realization in materials such as α -RuCl₃, Li₂IrO₃, and Na₂IrO₃ continue to present open questions about how the dynamics of a spin liquid are modified in the presence of non-Kitaev interactions as well as the presence of inhomogeneities. Here we use ²³Na nuclear magnetic resonance to probe both static and dynamical magnetic properties in single-crystal Na₂IrO₃. We find that the NMR shift follows the bulk susceptibility above 30 K but deviates from it below; moreover below T_N the spectra show a broad distribution of internal magnetic fields. Both of these results provide evidence for inequivalent magnetic sites at low temperature, suggesting inhomogeneities are important for the magnetism. The spin-lattice relaxation rate is isotropic and diverges at T_N , suggesting that the Kitaev cubic axes may control the critical quantum spin fluctuations. In the ordered state, we observe gapless excitations, which may arise from site substitution, emergent defects from milder disorder, or possibly be associated with nearby quantum paramagnetic states distinct from the Kitaev spin liquid.

DOI: 10.1103/PhysRevB.101.081101

In recent years there has been increasing interest in the so-called Kitaev materials $A_2 \text{IrO}_3$ (A = Na, Li), which are model systems for Kitaev honeycomb physics, similar to α -RuCl₃ and Li₂RhO₃ [1–5]. The Ir has electronic configuration $5d^5$, and a combination of spin-orbit coupling, Coulomb interactions, and crystal-field interactions give rise to a Mott insulating state with a gap of 340 meV [6]. Importantly, the j = 1/2 Ir spins in the honeycomb structure experience Ising interactions along different x, y, z directions with the three neighboring spins in the lattice. These couplings are strongly frustrated, and theory predicts an exotic spin-liquid ground state with itinerant, gapless Majorana fermion states [3]. In addition to the Kitaev interaction, higher-order Heisenberg terms are relevant in Na₂IrO₃, giving rise to long-range zigzag antiferromagnetic order of the Ir spins below 15 K [7-9]. At high temperatures, the magnetic susceptibility exhibits Curie-Weiss behavior with an effective moment close to that expected for spin 1/2 [10,11]. Diffuse magnetic x-ray scattering experiments have provided compelling evidence for the presence of significant bond directional interactions, which suggest that the Kitaev interactions indeed dominate the magnetic degrees of freedom [12].

The low-energy spin dynamics in Na₂IrO₃ and their relation to the relative size of the Kitaev and Heisenberg interaction terms have remained unclear, however. Complicating matters is the fact that disorder could potentially give rise to additional magnetic moments with their own low-energy dynamics. NMR is a powerful microscopic probe that can shed light on the low-temperature behavior of the iridates. The NMR shift, *K*, probes the intrinsic spin susceptibility. Disorder and extrinsic effects can dominate the bulk magnetic response, precluding a detailed understanding of the low-temperature behavior. Furthermore, the NMR spin-lattice

relaxation rate, T_1^{-1} , probes the dynamical spin susceptibility, providing information about the low-energy excitations that are present in the system.

NMR has played an important role in uncovering the physics of the related Kitaev honeycomb-lattice material, α -RuCl₃. In this system T_1^{-1} is strongly field and temperature dependent, reflecting the suppression of long-range order and the emergence of a field-induced quantum spin liquid above 9 T [13]. Both the bulk susceptibility, χ , and T_1^{-1} are strongly anisotropic in this material. Whether or not the field-induced phase exhibits a spin gap remains unclear, however [14,15]. The spin-liquid phase of the related compound H₃LiIr₂O₆ has also been investigated by NMR [16]. Li₂IrO₃ and Na₂IrO₃ have been studied less. Large single crystals of Li₂IrO₃ are difficult to grow; however, a mosaic of several submillimeter crystals has been studied, revealing similar behavior to α -RuCl₃ [17]. NMR and μ SR studies of polycrystalline Na₂IrO₃ have been reported recently which probe the phase diagram as a function of pressure and Li doping [18].

Here we report detailed 23 Na (I = 3/2) NMR studies of a high-quality single crystal of Na₂IrO₃, which reveal a broad static field distribution below 15 K, as well as a peak in T_1^{-1} associated with the critical dynamics of an antiferromagnetic transition. In the paramagnetic state, K is temperature dependent and anisotropic, similar to the bulk susceptibility. However, K does not track χ over the entire temperature range, but deviates below a temperature $T^* \sim 30$ K. Surprisingly, T_1^{-1} is isotropic, and in the ordered state the spin dynamics reveal no sign of the opening of a gap. Rather, $(T_1T)^{-1}$ remains constant as $T \to 0$, suggesting that fluctuations of the Ir moments persist deep in the long-range ordered state and that Na₂IrO₃ is located in close proximity to a quantum spin-liquid state. The presence of disorder, possibly

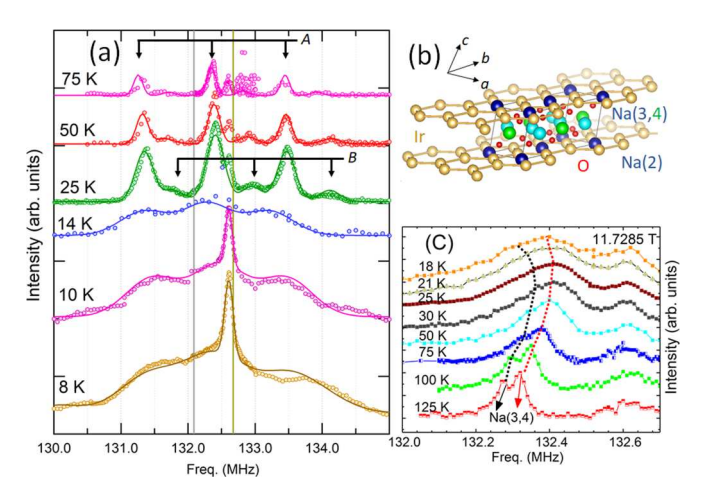


FIG. 1. (a) 23 Na spectra at fixed field $\mathbf{H}_0 \parallel c^*$ in Na₂IrO₃ at several different temperatures. The vertical line at 132.09 MHz corresponds to the Larmor frequency of 23 Na, and that at 132.67 MHz corresponds to the resonance frequency of metallic 63 Cu. The solid lines are fits as described in the text. (b) Structure of Na₂IrO₃, indicating the three Na sites in the unit cell, and the honeycomb structure of the iridium atoms. Note that c^* is normal to the planes, whereas c is not. (c) Detailed spectra of the Na(3) and Na(4) central transitions at several temperatures, showing the resolution of two separate peaks.

from Na-Ir site substitutions or the presence of stacking faults, provides a consistent explanation for these observations.

Single crystals of Na₂IrO₃ were prepared by mixing elemental Ir (99.9% purity; BASF) with Na₂CO₃ (99.9999% purity; Alfa-Aesar) in a 1:1.05 molar ratio. The mixture was ground for several minutes, then pressed into a pellet at approximately 3000 psi. The pellet was then warmed in a furnace to 1050 °C and held at temperature for 48 h, before being cooled to 900 °C over 24 h and then furnace cooled. Single crystals more than one square millimeter were then collected from the surface of the pellet. A crystal of dimensions 1.1 mm×0.9 mm×0.07 mm was selected and oriented with magnetic field $H_0 = 11.73 \text{ T}$ applied parallel and perpendicular to the c^* direction (normal to the ab plane). NMR experiments were performed at a fixed field for temperatures between 4 and 300 K. ²³Na (I = 3/2, $\gamma = 11.2625$ MHz/T, 100% abundance) NMR spectra were collected by a homebuilt auto-tuning and matching NMR probe over broad frequency ranges. Silver wire was used for the NMR coil to avoid overlap between the ⁶³Cu and ²³Na resonances. ²³Na spectra were acquired by collecting spin echoes as a function of frequency, and spin-lattice relaxation rate measurements were conducted by observing the spin echo following an inversion pulse at the central transition.

Figure 1 shows ²³Na NMR spectra collected at several representative temperatures. There are three nonequivalent Na sites in Na₂IrO₃ [see Fig. 1(b)], each described by the Hamiltonian $\mathcal{H} = \gamma \hbar \hat{\mathbf{I}} \cdot (1 + \mathbf{K}) \cdot \mathbf{H}_0 + \frac{\hbar \nu_{zz}}{6} [3\hat{I}_z^2 - \hat{I}^2 + \eta(\hat{I}_x^2 - \hat{I}_y^2)]$, where $\eta = (\nu_{xx} - \nu_{yy})/\nu_{zz}$, and $\nu_{\alpha\alpha}$ are the eigenvalues of the electric field gradient (EFG) tensor, and \mathbf{K} is the NMR shift tensor [19]. \mathbf{H}_0 is not necessarily parallel to any of the principle directions of either the NMR shift or the EFG tensors. At high temperatures the spectra are considerably

narrow and the satellite structure is clearly evident. There is also a temperature-independent background resonance at 132.67 MHz from metallic Cu. Below 50 K, a second set of resonances emerges, and below 14 K the spectra become significantly broader, with one narrow peak centered at 132.6 MHz. The narrow peak is temperature independent, and we ascribe this to a spurious background signal from ⁶³Cu in the probe. The broad spectra arise from the ²³Na in the crystal, which experience a range of internal magnetic fields in the magnetically ordered state.

We fit the spectra in Fig. 1(a) to extract the NMR shifts, K, the quadrupolar splittings, $v_{c^*c^*}$, and the second moment, σ , for two ²³Na sites, tentatively identified as sites A and B. The fitting was performed by exact diagonalization and accounts for the three quadrupolar-split resonances for both sites simultaneously. Site A exhibits a higher intensity with quadrupolar splitting $\nu_{c^*c^*}(A) = 1.056 \pm 0.003$ MHz and NMR shift $K(A) = 0.242 \pm 0.001\%$. The spectrum for site B is approximately 1/3 in intensity, with a larger $v_{c^*c^*}(B) = 1.16 \pm 1.16$ 0.02 MHz and larger NMR shift $K(B) = 0.65 \pm 0.01\%$. At lower temperatures, the central transition for site A splits into two separate peaks with slightly different NMR shifts, as shown in Fig. 1(c). We therefore identify site A as the Na(3) and Na(4) sites, located between the Ir layers, and site B as the Na(2), located within the Ir planes. This assignment is supported by point charge calculations of the EFG for the three sites, which indicate a slightly larger EFG at the Na(2) site. The EFG for the two interplanar sites, Na(3) and Na(4), is similar, but they appear to have slightly different NMR shifts. We are unable to determine which site corresponds to which shift, but for concreteness we assign Na(3) to the lower NMR shift. At higher temperature, the shifts and quadrupolar splittings for these two sites are not distinct enough to resolve. We find that the EFG parameters change by less than 5% with temperature in the paramagnetic phase.

Figures 2(a) and 2(b) display the temperature dependence of the second moment and NMR shift versus temperature for both sites. The linewidth increases with decreasing temperature, but increases by a factor of 3 at the Na(2) site below 14 K. This increase reflects the presence of local internal magnetic fields present at the Na(2) site due to the onset of static magnetic order. The fact that the spectra do not reveal any sharp peaks below T_N but rather are broad and featureless indicates a distribution of internal fields. Similar results have been also observed in the ordered phase of RuCl₃ [13]. This observation suggests incommensurate magnetic order; however, neutron and x-ray scattering studies indicate a commensurate zigzag antiferromagnetic order [7,9], and muon time spectra exhibit oscillations indicating a well-defined static internal field at the muon site, rather than a broad distribution of fields as expected for incommensurate order [20]. A possible explanation for this discrepancy is substitutional disorder among the Na and Ir lattice sites, as discussed below. Note that the Na is likely coupled to several nearest-neighbor Ir spins through a complex set of hyperfine couplings. As a result, even a small level of disorder can quickly lead to a broad distribution of static hyperfine fields, both in terms of magnitude and direction [21]. In the paramagnetic state, we find that the temperature dependence of the second moment can be fit empirically to $\sigma_1(T) = A + Be^{-T/T_0}$, with A = 0.048 MHz,

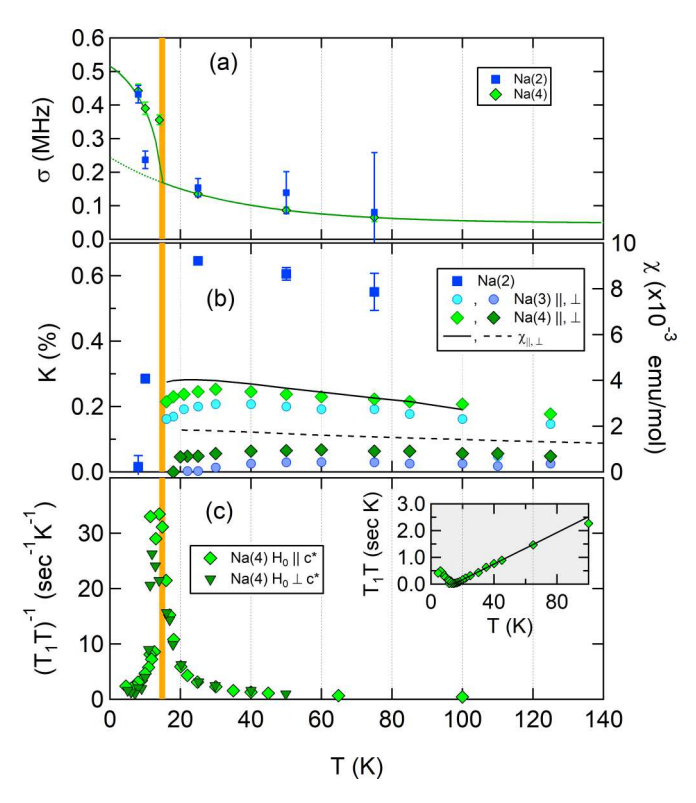


FIG. 2. (a) Second moments of the Gaussian spectral functions used to fit the data shown in Fig. 1 versus temperature. The solid and dashed lines are fits as described in the text. (b) NMR shifts of three sites and the bulk magnetic susceptibility (solid line) versus temperature. (c) $(T_1T)^{-1}$ measured at the Na(3) and Na(4) sites as a function of temperature, for both $\mathbf{H}_0 \parallel c^*$ and $\mathbf{H}_0 \perp c^*$. The solid vertical orange line indicates T_N . Inset: T_1T versus T for $\mathbf{H}_0 \parallel c^*$, with a linear fit (solid line), indicating a divergence at $T_N = 14.3 \pm 0.1$ K.

B = 0.196 MHz, and $T_0 = 30.0$ K. Below T_N we include an extra mean-field broadening term, $\sigma(T) = \sigma_1(T) + \sigma_2(T)$, where $\sigma_2(T) = \sigma_0 \sqrt{1 - (T/T_N)^2}$, with $\sigma_0 = 0.27$ MHz, and $T_N = 14.3$ K. This fit is shown as a solid line in Fig. 2(a).

The NMR shift shown in Figs. 2(b) and 3(a) is compared with the bulk magnetic susceptibility, χ , measured for fields both parallel and perpendicular to the c^* direction. For both

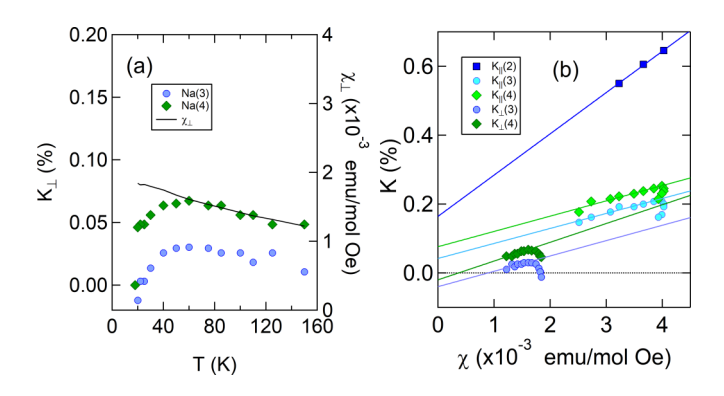


FIG. 3. (a) NMR shifts and magnetic susceptibility (solid line) versus temperature for the field-oriented perpendicular to c^* . (b) NMR shifts versus susceptibility for both field directions. The solid lines are fits to the high-temperature data, as described in the text, with fitting parameters detailed in Table I.

TABLE I. Hyperfine parameters from fits to the high-temperature data as shown in Fig. 3.

Site	K_{\parallel}^{0} (%)	K_{\perp}^{0} (%)	A_{\parallel} (kOe/ μ_B)	A_{\perp} (kOe/ μ_B)
Na(2)	0.06 ± 0.02		6.70 ± 0.26	
Na(3)	0.04 ± 0.01	-0.04 ± 0.01	2.43 ± 0.30	2.49 ± 0.40
Na(4)	0.08 ± 0.02	-0.02 ± 0.01	2.48 ± 0.50	3.05 ± 0.38

directions, K increases with decreasing temperature down to a maximum \sim 30 K, and then decreases below. The NMR shift derives from the hyperfine coupling between the ²³Na nuclear spins and the Ir electron moments, and the NMR shift should be proportional to χ as $K = A\chi + K_0$, where A is the hyperfine coupling constant and K_0 is a temperature-independent constant. As seen in Fig. 2(b), K and χ exhibit similar behavior at high temperature, but below this temperature Kand χ no longer track one another. This anomalous behavior is clearly evident in Fig. 3(b), where K is plotted versus χ for both field directions. At high temperatures K and χ are linearly proportional with hyperfine constants given in Table I. These values are about an order of magnitude larger than the direct dipolar coupling between the Na nuclei and the Ir electron spins (on the order of $0.5 \text{ kOe}/\mu_B$), and are consistent with a transferred hyperfine coupling due to wave-function overlap. Given this value of the hyperfine field, we can estimate the magnitude of the ordered moments as $S_0 \approx \sigma_0/\gamma A \sim$ $0.1\mu_B/\text{Ir}$. This order of magnitude is consistent with neutronscattering measurements that indicate $0.22\mu_B/\text{Ir}$.

The breakdown of the linear $K-\chi$ relationship at low temperature is puzzling. In heavy fermions, an NMR shift anomaly usually reflects the onset of coherence [22,23]; however, Na₂IrO₃ is insulating and there should be no such effect. It is possible that there are different hyperfine couplings to the orbital and spin moments of the Ir, but the spin and orbital susceptibilities will exhibit the same temperature dependence due to the strong spin-orbit coupling. In this case, the $K-\chi$ relationship will reflect a renormalized effective hyperfine coupling [24], but will not exhibit an anomaly as we observe. Such an anomaly usually indicates the presence of multiple magnetically active sites with different temperature dependences. Substitutional disorder, with some fraction of the Ir sites located at the Na sites rather than in the honeycomblattice structure, could therefore explain this behavior. A similar breakdown of the K- χ relationship has also been observed in RuCl₃ [13].

In addition to the spectra we also measured the spin-lattice relaxation rate, T_1^{-1} , at the central transition of the Na(3,4) sites for both field orientations. The magnetization recovery was fit to a stretched exponential appropriate for the central transition of a spin-3/2 nucleus: $M(t) = M_0[1 - 2f(\frac{9}{10}e^{-(6t/T_1)^{\beta}} + \frac{1}{10}e^{-(t/T_1)^{\beta}})]$ where M_0 is the equilibrium nuclear magnetization, f is the inversion fraction, and β is the stretched exponent. We find that $\beta \approx 0.7$ and is temperature independent. Figure 2(c) displays $(T_1T)^{-1}$ as a function of temperature. This quantity probes the dynamical spin susceptibility through the relationship

$$\left(\frac{1}{T_1 T}\right)_{\alpha} = \gamma^2 k_B T \lim_{\omega \to 0} \sum_{\mathbf{q}, \beta \neq \alpha} \mathcal{F}_{\alpha\beta}(\mathbf{q}) \frac{\mathrm{Im} \chi_{\alpha\beta}(\mathbf{q}, \omega)}{\hbar \omega}, \quad (1)$$

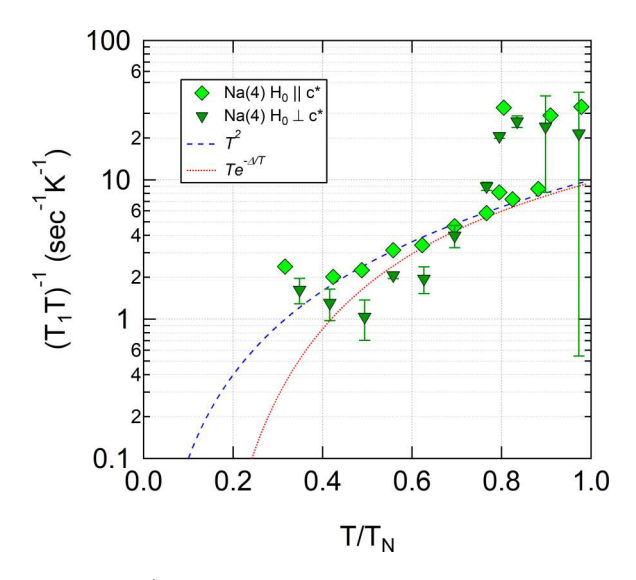


FIG. 4. $(T_1T)^{-1}$ versus T for $\mathbf{H}_0 \| c^* (\spadesuit)$ and $\mathbf{H}_0 \bot c^* (\blacktriangledown)$ below T_N .

where $\mathcal{F}_{\alpha\beta}(\mathbf{q})$ are form factors that depend on the hyperfine coupling tensor, $\chi_{\alpha\beta}(\mathbf{q},\omega)$ is the dynamical magnetic susceptibility, and α , $\beta = \{x, y, z\}$ [25]. The large peak in $(T_1T)^{-1}$ reflects the slowing down of critical fluctuations near T_N . As shown in the inset of Fig. 2(c), T_1T varies linearly, and a linear fit indicates this quantity vanishes at $T_N = 14.3 \text{ K. Surprisingly, } (T_1 T)^{-1} \text{ appears to be isotropic}$ over the entire temperature range, despite the anisotropy observed in K and the static susceptibility [Figs. 2(b) and 3]. Both anisotropy in the form factors and in the dynamical spin susceptibility itself can contribute to the anisotropy of $(T_1T)^{-1}$. However, the hyperfine couplings given in Table I vary by at most 20% for the two field orientations, thus the critical spin fluctuations themselves must be largely isotropic in the paramagnetic state. This result contrasts with NMR observations in α -RuCl₃ [13], but agrees with magnetic x-ray scattering results in the paramagnetic state, where the zigzag correlations decrease isotropically with increasing the temperature [12]. The fact that the spin fluctuations in Na₂IrO₃ show no difference between in-plane and out-of-plane magnetic fields suggests that, despite the strong spin-orbit coupling evident in the magnetic order, the same strong spin-orbit coupling conspires to produce a symmetry in the critical fluctuations that is indistinguishable from spherical symmetry, consistent with the isotropy of the Kitaev cubic axes.

Figure 4 displays $(T_1T)^{-1}$ versus temperature below T_N . It is well established that in a three-dimensional conventional magnetic insulator the spin-lattice relaxation rate exhibits either thermally activated behavior, $(T_1T)^{-1} \propto Te^{-\Delta/T}$, or power-law relaxation, $(T_1T)^{-1} \propto T^{\alpha}$, where $\alpha=2$ or 4 for two-magnon or three-magnon scattering [26,27]. We fit the data to both expressions, but as seen in Fig. 4 neither expression captures the behavior well. For an ideal Kitaev spin model, the NMR spin-lattice relaxation rate is expected to exhibit activated behavior, $T_1^{-1} \sim e^{-\Delta/k_BT}$, where Δ is the spin gap [28,29]. For the more generic case of a gapless Kitaev quantum spin liquid on a honeycomb lattice, $T_1^{-1} \propto T^3$ [30]. However, neither of these cases adequately captures our

observations either. Surprisingly, the data in Fig. 4 approach a constant as $T \to 0$. This result is surprising because at T = 0 all of the fluctuations should be frozen out. $(T_1T)^{-1} = \text{const}$ suggests the presence of a finite density of states in a conductor, but Na₂IrO₃ is a Mott insulator with a band gap of 300 meV so relaxation by itinerant charges can be ruled out. Observations in similar materials reveal different trends. In polycrystalline samples of the two-dimensional honeycomb material Li₂RhO₃, $T_1^{-1} \propto T^{2.2}$ [31]. In RuCl₃, T_1^{-1} exhibits qualitatively similar behavior at low fields, with a peak at T_N and decreasing T_1^{-1} below; however, at high fields T_1^{-1} is dramatically suppressed as the magnetism is suppressed and a spin gap emerges [13].

The presence of a small population of minority Ir spins located at the Na sites may offer an explanation for the gapless excitations we observe at low temperatures in the antiferromagnetic phase, consistent with the breakdown of the K- χ relationship. Because these minority spins may not order, they would continue to fluctuate and can contribute to the spin-lattice relaxation of the Na nuclei. Substitutional disorder is not uncommon in these materials, and structural refinement studies have indicated that up to 35% of the Na(2) sites can be occupied by Ir [9].

An alternative possibility is that layer stacking faults may be present which could be correlated with each other in complicated ways. The net result is that some layers could magnetically interact with each other enough to give different regions of the crystal with somewhat different magnetic properties. Though they all undergo the same three-dimensional T_N transition, the resulting regions would have different magnetic sites across the crystal experiencing different internal fields. A related possibility is that stacking faults could produce inhomogeneous electric fields that can then change magnetic interaction energies; in quantum paramagnets such energy randomness can give rise to topological defects carrying spin-1/2 moments, with unusual low-energy dynamics, and it is conceivable that some such magnetic defects can arise from energy randomness also in this strongly frustrated, albeit ordered, magnet [32,33].

In conclusion, we have found that the Na NMR spectrum exhibits a shift anomaly below ~30 K, and a significant broadening below T_N associated with a broad distribution of local internal fields in the antiferromagnetic state, despite independent observations of commensurate ordering. We attribute these effects to Ir-Na substitutional disorder, which may give rise to a subset of Ir spins that exhibit different magnetic behavior than those in the honeycomb lattice. The surprising lack of anisotropy in T_1^{-1} in the paramagnetic phase suggests that isotropic spin fluctuations are driven by Kitaev interaction. Furthermore, T_1^{-1} data reveal gapless excitations deep in the ordered state, which may also arise from disorder. Although this type of substitutional disorder is particular to the A₂IrO₃ family, similar phenomena have been observed in RuCl₃ and it is important to account for the consequences of such a distribution into two subsystems to fully understand the nature of the low-energy excitations within the quantum spin-liquid phase of related materials. Further studies at lower temperature may shed important light on the nature of these excitations.

We acknowledge helpful discussions with T. Kissikov and B. Bush. This research is supported by the Deutsche Forschungsgemeinschaft (DFG) through SFB 1143 for the project C02. Work at UC Davis was supported by the NSF

under Grants No. DMR-1506961 and No. DMR-1807889. Work by J.G.A. was supported by the Department of Energy, Office of Basic Energy Sciences, Early Career program under Contract No. DE-AC02-05CH11231.

- [1] S. Trebst, Kitaev materials, arXiv:1701.07056.
- [2] P. Gegenwart and S. Trebst, Kitaev matter, Nat. Phys. 11, 444 (2015).
- [3] M. Hermanns, I. Kimchi, and J. Knolle, Physics of the Kitaev model: Fractionalization, dynamic correlations, and material connections, Annu. Rev. Condens. Matter Phys. 9, 17 (2018).
- [4] G. Jackeli and G. Khaliullin, Mott Insulators in the Strong Spin-Orbit Coupling Limit: From Heisenberg to a Quantum Compass and Kitaev Models, Phys. Rev. Lett. 102, 017205 (2009).
- [5] H. Takagi, T. Takayama, G. Jackeli, G. Khaliullin, and S. E. Nagler, Concept and realization of Kitaev quantum spin liquids, Nat. Rev. Phys. 1, 264 (2019).
- [6] R. Comin, G. Levy, B. Ludbrook, Z.-H. Zhu, C. N. Veenstra, J. A. Rosen, Y. Singh, P. Gegenwart, D. Stricker, J. N. Hancock, D. van der Marel, I. S. Elfimov, and A. Damascelli, Na₂IrO₃ as a Novel Relativistic Mott Insulator with a 340-meV Gap, Phys. Rev. Lett. 109, 266406 (2012).
- [7] J. Chaloupka, G. Jackeli, and G. Khaliullin, Zigzag Magnetic Order in the Iridium Oxide Na₂IrO₃, Phys. Rev. Lett. 110, 097204 (2013).
- [8] X. Liu, T. Berlijn, W.-G. Yin, W. Ku, A. Tsvelik, Y.-J. Kim, H. Gretarsson, Y. Singh, P. Gegenwart, and J. P. Hill, Long-range magnetic ordering in Na₂IrO₃, Phys. Rev. B 83, 220403(R) (2011).
- [9] F. Ye, S. Chi, H. Cao, B. C. Chakoumakos, J. A. Fernandez-Baca, R. Custelcean, T. F. Qi, O. B. Korneta, and G. Cao, Direct evidence of a zigzag spin-chain structure in the honeycomb lattice: A neutron and x-ray diffraction investigation of single-crystal Na₂IrO₃, Phys. Rev. B 85, 180403(R) (2012).
- [10] Y. Singh, S. Manni, J. Reuther, T. Berlijn, R. Thomale, W. Ku, S. Trebst, and P. Gegenwart, Relevance of the Heisenberg-Kitaev Model for the Honeycomb Lattice Iridates A₂IrO₃, Phys. Rev. Lett. 108, 127203 (2012).
- [11] Y. Singh and P. Gegenwart, Antiferromagnetic Mott insulating state in single crystals of the honeycomb lattice material Na₂IrO₃, Phys. Rev. B **82**, 064412 (2010).
- [12] S. H. Chun, J.-W. Kim, J. Kim, H. Zheng, C. C. Stoumpos, C. D. Malliakas, J. F. Mitchell, K. Mehlawat, Y. Singh, Y. Choi, T. Gog, A. Al-Zein, M. M. Sala, M. Krisch, J. Chaloupka, G. Jackeli, G. Khaliullin, and B. J. Kim, Direct evidence for dominant bond-directional interactions in a honeycomb lattice iridate Na₂IrO₃, Nat. Phys. 11, 462 (2015).
- [13] S.-H. Baek, S.-H. Do, K.-Y. Choi, Y. S. Kwon, A. U. B. Wolter, S. Nishimoto, J. van den Brink, and B. Büchner, Evidence for a Field-Induced Quantum Spin Liquid in α-RuCl₃, Phys. Rev. Lett. 119, 037201 (2017).
- [14] N. Janša, A. Zorko, M. Gomilšek, M. Pregelj, K. W. Krämer, D. Biner, A. Biffin, C. Rüegg, and M. Klanjšek, Observation of two types of fractional excitation in the Kitaev honeycomb magnet, Nat. Phys. 14, 786 (2018).
- [15] J. Zheng, K. Ran, T. Li, J. Wang, P. Wang, B. Liu, Z.-X. Liu, B. Normand, J. Wen, and W. Yu, Gapless Spin Excitations

- in the Field-Induced Quantum Spin Liquid Phase of α -RuCl₃, Phys. Rev. Lett. **119**, 227208 (2017).
- [16] K. Kitagawa, T. Takayama, Y. Matsumoto, A. Kato, R. Takano, Y. Kishimoto, S. Bette, R. Dinnebier, G. Jackeli, and H. Takagi, A spin-orbital-entangled quantum liquid on a honeycomb lattice, Nature (London) 554, 341 (2018).
- [17] M. Majumder, F. Freund, T. Dey, M. Prinz-Zwick, N. Büttgen, Y. Skourski, A. Jesche, A. A. Tsirlin, and P. Gegenwart, Anisotropic temperature-field phase diagram of single crystalline β-Li₂IrO₃: Magnetization, specific heat, and ⁷Li NMR study, Phys. Rev. Mater. 3, 074408 (2019).
- [18] G. Simutis, N. Barbero, K. Rolfs, P. Leroy-Calatayud, K. Mehlawat, R. Khasanov, H. Luetkens, E. Pomjakushina, Y. Singh, H.-R. Ott, J. Mesot, A. Amato, and T. Shiroka, Chemical and hydrostatic-pressure effects on the Kitaev honeycomb material Na₂IrO₃, Phys. Rev. B 98, 104421 (2018).
- [19] C. P. Slichter, Principles of Nuclear Magnetic Resonance, 3rd ed. (Springer-Verlag, Berlin, 1992).
- [20] S. K. Choi, R. Coldea, A. N. Kolmogorov, T. Lancaster, I. I. Mazin, S. J. Blundell, P. G. Radaelli, Y. Singh, P. Gegenwart, K. R. Choi, S.-W. Cheong, P. J. Baker, C. Stock, and J. Taylor, Spin Waves and Revised Crystal Structure of Honeycomb Iridate Na₂IrO₃, Phys. Rev. Lett. 108, 127204 (2012).
- [21] A. P. Dioguardi, N. apRoberts-Warren, A. C. Shockley, S. L. Bud'ko, N. Ni, P. C. Canfield, and N. J. Curro, Local magnetic inhomogeneities in Ba(Fe_{1-x}Ni_x)₂As₂ as seen via ⁷⁵As NMR, Phys. Rev. B **82**, 140411(R) (2010).
- [22] N. J. Curro, Nuclear Magnetic Resonance as a Probe of Strongly Correlated Electron Systems (Springer, New York, 2014), pp. 1–30
- [23] N. J. Curro, Nuclear magnetic resonance in the heavy fermion superconductors, Rep. Prog. Phys. 72, 026502 (2009).
- [24] D. M. Nisson and N. J. Curro, Nuclear magnetic resonance Knight shifts in the presence of strong spin-orbit and crystalfield potentials, New J. Phys. 18, 073041 (2016).
- [25] T. Moriya, The effect of electron-electron interaction on the nuclear spin relaxation in metals, J. Phys. Soc. Jpn. 18, 516 (1963).
- [26] D. Beeman and P. Pincus, Nuclear spin-lattice relaxation in magnetic insulators, Phys. Rev. 166, 359 (1968).
- [27] M. Günther, S. Kamusella, R. Sarkar, T. Goltz, H. Luetkens, G. Pascua, S.-H. Do, K.-Y. Choi, H. D. Zhou, C. G. F. Blum, S. Wurmehl, B. Büchner, and H.-H. Klauss, Magnetic order and spin dynamics in La₂O₂Fe₂OSe₂ probed by ⁵⁷Fe Mössbauer, ¹³⁹La MNR, and muon-spin relaxation spectroscopy, Phys. Rev. B 90, 184408 (2014).
- [28] J. Knolle, D. L. Kovrizhin, J. T. Chalker, and R. Moessner, Dynamics of a Two-Dimensional Quantum Spin Liquid: Signatures of Emergent Majorana Fermions and Fluxes, Phys. Rev. Lett. 112, 207203 (2014).
- [29] J. Knolle, D. L. Kovrizhin, J. T. Chalker, and R. Moessner, Dynamics of fractionalization in quantum spin liquids, Phys. Rev. B 92, 115127 (2015).

- [30] X.-Y. Song, Y.-Z. You, and L. Balents, Low-Energy Spin Dynamics of the Honeycomb Spin Liquid Beyond the Kitaev Limit, Phys. Rev. Lett. **117**, 037209 (2016).
- [31] P. Khuntia, S. Manni, F. R. Foronda, T. Lancaster, S. J. Blundell, P. Gegenwart, and M. Baenitz, Local magnetism and spin dynamics of the frustrated honeycomb rhodate Li₂RhO₃, Phys. Rev. B **96**, 094432 (2017).
- [32] I. Kimchi, A. Nahum, and T. Senthil, Valence Bonds in Random Quantum Magnets: Theory and Application to YbMgGaO₄, Phys. Rev. X 8, 031028 (2018).
- [33] I. Kimchi, J. P. Sheckelton, T. M. McQueen, and P. A. Lee, Scaling and data collapse from local moments in frustrated disordered quantum spin systems, Nat. Commun. 9, 4367 (2018).